REPORT DOCUMENTATION PAGE

AFRL-SR-BL-TR-02-

0147

1. AGENCY USE ONLY (Leave Blank)	2. REPORT DATE	3. REPORT TYPE AND DATES COVERED
	3/29/02	Final Technical 01 Sept 97 - 31 Aug 01

4. TITLE AND SUBTITLE

Novel All-Fiber Devices Based on the Electro-Optic Effect in Poled Fused Silica

5. FUNDING NUMBERS

AFOSR F49620-97-1-0374

6. AUTHOR(S)

Ravinder Jain

7. PERFORMING ORGANIZATION NAME(S) AND ADDRESS(ES)

The University of New Mexico
Center for High Technology Materials,
1313 Goddard SE
Albuquerque, NM 87106

8. PERFORMING ORGANIZATION REPORT NUMBER

FT349011B

9. SPONSORING / MONITORING AGENCY NAME(S) AND ADDRESS(ES)

AFOSR/NE
801 North Randolph Street
Arlington, VA 22203-1977

10. SPONSORING / MONITORING AGENCY REPORT NUMBER

11. SUPPLEMENTARY NOTES

The views, opinions and/or findings contained in this report are those of the author(s) and should not be construed as an official Defense Advanced Research Projects Agency position, policy or decision, unless so designated by other documentation.

12 a. DISTRIBUTION / AVAILABILITY STATEMENT

Approved for public release; distribution unlimited.

12 b. DISTRIBUTION CODE

13. ABSTRACT (Maximum 200 words)

This report describes research on the study of novel all-fiber devices based on the electro-optic effect in poled fused silica. The focus of the current work was on electro-optically tunable all-fiber waveplates, since they form the basis of the design of a large array of novel all-fiber devices, including all-fiber modulators and all-fiber tunable filters for WDM telecommunications systems. The all-fiber waveplates studied are applicable for the design of in-line phase retarders, in-line polarization controllers, and in-line tunable fiber Bragg gratings, as elucidated in this study. Unfortunately, the highest second-order nonlinearities obtained were <0.04 pm/V, necessitating operating voltages of several kilovolts, and limiting their applicability to practical telecom devices. Further studies need to be conducted to reliably and reproducibly increase the observed electro-optic nonlinearities before practical implementation of the novel all-fiber devices that were the key targets of the present work.

20020509 017

14. SUBJECT TERMS

All-fiber Devices, Electro-optic Fibers, Poled Fibers, Poled Fused Silica

15. NUMBER OF PAGES

27

16. PRICE CODE

NSP

17. SECURITY CLASSIFICATION OR REPORT	18. SECURITY CLASSIFICATION ON THIS PAGE	19. SECURITY CLASSIFICATION OF ABSTRACT	20. LIMITATION OF ABSTRACT
UNCLASSIFIED	UNCLASSIFIED	UNCLASSIFIED	UL

Final Technical Report on AFOSR-AASERT Grant

AFOSR Grant # F49620 – 97-1-0374

Novel All-Fiber Devices Based on the Electro-Optic Effect in Poled Fused Silica

Keywords: All-fiber Devices, Electro-optic Fibers, Poled Fibers, Poled Fused Silica

ABSTRACT

This report describes research on the study of novel all-fiber devices based on the electro-optic effect in poled fused silica. The focus of the current work was on electro-optically tunable all-fiber waveplates, since they form the basis of the design of a large array of novel all-fiber devices, including all-fiber modulators and all-fiber tunable filters for WDM telecommunications systems. The all-fiber waveplates studied are applicable for the design of in-line phase retarders, in-line polarization controllers, and in-line tunable fiber Bragg gratings, as elucidated in this study. Unfortunately, the highest second-order nonlinearities obtained were <0.04 pm/V, necessitating operating voltages of several kilovolts, and limiting their applicability to practical telecom devices. Further studies need to be conducted to reliably and reproducibly increase the observed electro-optic nonlinearities before practical implemenation of the novel all-fiber devices that were the key targets of the present work.

Key students supported by this grant:

Brad Austin, Anthony Bilotto, Chris Kletecka, Chris Padilla, Jimmie Wolf.

Final Technical Report on AFOSR-AASERT Grant

AFOSR Grant # F49620 – 97-1-0374

Novel All-Fiber Devices Based on the Electro-Optic Effect in Poled Fused Silica

A. Introduction and Background

A.1. Motivation

The control of the state of light polarization in an optical fiber is an important issue that impacts the performance of modelocked fiber lasers, narrow linewidth fiber lasers, and several interferometric sensing applications. Standard single mode fibers usually do not preserve the state of polarization because of spurious birefringence in the fiber. Moreover, since the birefringence can change with the physical environment of the fiber, one generally observes random fluctuations in the output polarization of the fiber [1]. One approach for circumventing this problem is to use a polarization preserving fiber that has an intrinsic birefringence much larger than the spurious birefringence. But, such a large birefringence and the resultant phase delay between the two eigenmodes of the fiber is undesirable for certain applications such as the detection of magnetic fields and electric currents through the Faraday effect [2]. A more attractive, powerful alternative approach is that of using polarization controllers to tailor the polarization to the desired state.

Polarization controllers based on a multiple cascade of alternating TE-TM polarization converter and TE/TM phase shifter sections in $LiNbO_3$ have been demonstrated previously [3,4]. Although excellent results have been achieved using this integrated optic approach, an all-fiber polarization controller is more desirable for

realizing "monolithic" all-fiber lasers. Towards this end, all-fiber polarization controllers based on stress-induced birefringence due to twisting, bending or squeezing the fiber have been demonstrated [5]. Popular among them is the device demonstrated by Lefevre [6], which employs a simple configuration using the stress birefringence induced by bending the fiber. Based on the bending radius (R) and the number of turns (N) of the fiber, half-waveplates or quarter-waveplates can be realized according to the relation,

$$\delta n.2\pi.N.R = \frac{\lambda}{m} \qquad \ldots (1)$$

where δn is the magnitude of the stress-induced birefringence and m is an even integer. By rotating the axis of the coil, one can change the optical axis of the waveplate. Using two quarter-waveplates to control the ellipticity of the light polarization and one half-waveplate sandwiched in between the quarter-waveplates to control the orientation, any desired output polarization can be achieved for a given input polarization [6].

The polarization controllers discussed above are bulky, cumbersome to handle and susceptible to environmental variations. To circumvent these problems, all-fiber compact polarization controllers without any moving parts are needed. Such polarization controllers can be achieved using poled fiber sections, which is a topic of discussion in this report.

A.2. Poling of Glasses and Fibers:

When certain materials are subjected to an external electric field, their optical properties are modified. This is caused by forces that distort the position, orientation, or

shape of the molecules constituting the material. The electro-optic effect is the change in the refractive index of a material due to the application of an electric field. The electro-optic effect affords a convenient and widely used means of controlling the phase or intensity of the optical radiation and as such is applicable to the impression of information on to optical beams, optical beam deflection, and spectral tunable filters.

The origin of the electro-optic effect can be traced back to a nonlinear polarization response, P(t), of the material due to an applied electric field, E(t). The nonlinear polarization response [7] can be expressed as

$$\begin{aligned} P(t) &= \chi^{(1)}E(t) + \chi^{(2)}E^2(t) + \chi^{(3)}E^3(t) + \chi^{(4)}E^4(t) + ... \\ &= E(t) \,.\, [\chi^{(1)} + \chi^{(2)}E(t) + \chi^{(3)}E^2(t) + \chi^{(4)}E^3(t) + ...] \qquad ... (2) \end{aligned}$$

where $\chi^{(1)}$ is the first-order susceptibility, $\chi^{(2)}$ is the second-order susceptibility, $\chi^{(3)}$ is the third-order susceptibility, and so on.

In most practical applications of the electro-optic effect, the applied electric field is small compared with the electric field inside the atom (typically of the order of 10^{10} V/m). As a result, in Eq. (2) the quadratic effect (through $\chi^{(3)}$) is expected to be small compared to the linear effect (through $\chi^{(2)}$) and is often neglected when the linear effect is present. However, in materials with centrosymmetric structure, the linear electro-optic effect vanishes and the quadratic effect becomes the dominant phenomenon. Such is the case of silica-based glass, an ubiquitous material that plays an important role in our everyday life including communications and sensing. Fused silica glass is a dominant material in optoelectronics largely because of its low fabrication cost compared to

crystalline materials, and its superior optical properties such as high transparency and high damage threshold.

In order to induce a second-order nonlinearity in fused silica glass, the centrosymmetry of the material must be broken. This could be achieved by applying a large electric field across the glass structure either by itself or in combination with heat or ultraviolet radiation. This process, known commonly as poling, leads to the creation of a "permanent" second-order nonlinearity and has been a researched by several groups during the last two decades. However, the poled glass research has gained significant momentum only after the pioneering work [8] at UNM, in which second-order nonlinearities of ~1 pm/V were demonstrated using a thermal-assisted poling process.

Although the thermal poling process, in which the glass sample is heated to ~260°C while a large electric field is applied, is the most popular one till date other poling processes are also promising. These processes include the UV-assisted poling process [9], the corona poling process [10], and the ion implantation process [11]. The UV-assisted poling process is believed to rely on defect formation in germanosilicate glasses upon UV irradiation (193 nm) and the reorientation of the defects (GeE' centers) under the influence of the electric field [12]. This process is reported to have yielded the highest second order nonlinearity (~6 pm/V) in fused silica. However, subsequent reports [13] have stated the nonlinearity decayed with a time constant of ~280 days at 15°C. This decay is attributed to the low activation energy (0.41 eV) of the defects responsible for the nonlinearity. Furthermore, the above results have not been reproducible by other

research groups. Hence this technology needs to be researched further before it becomes commercially viable.

The corona poling process uses a pointed electrode held near the sample surface to orient dipoles in the sample at relatively low temperatures (up to 100°C) for several hours [14]. This process has the advantage of the electrode not being in contact with the sample and the use of lower temperatures while achieving nonlinearities comparable to thermal poling. But, the nonlinearity decayed quickly within a few hours, followed by a slower decay over several days [15] and hence is not yet attractive. Poling has also been achieved by electron implantation in lead silicate glasses using a focused electron beam [11]. Electron implantation has the advantage of high spatial resolution that is necessary for creating quasi-phase-matching (QPM) structures and complex patterns for advanced electro-optic modulators. Using this technique, $\chi^{(2)}$ values of 0.7 pm/V was demonstrated in lead silicate glasses, but the technique did not work for fused silica.

Amongst the above poling methods, thermal poling appears to be the most stable and reliable method for inducing a second-order nonlinearity in fused silica. The work described in the following sections was all performed using the thermal poling method. A simple model for understanding the dynamics of the thermal poling process is described as follows: as shown in Fig. 1, initially all the mobile charges in the glass sample feel an uniform force due to an electric field, E_0 corresponding to the ratio of the applied voltage (V) and the thickness (D) of the sample. Then, cations such as Na^+, K^+, Li^+ etc. start moving towards the cathode, leaving behind a depletion region consisting of an

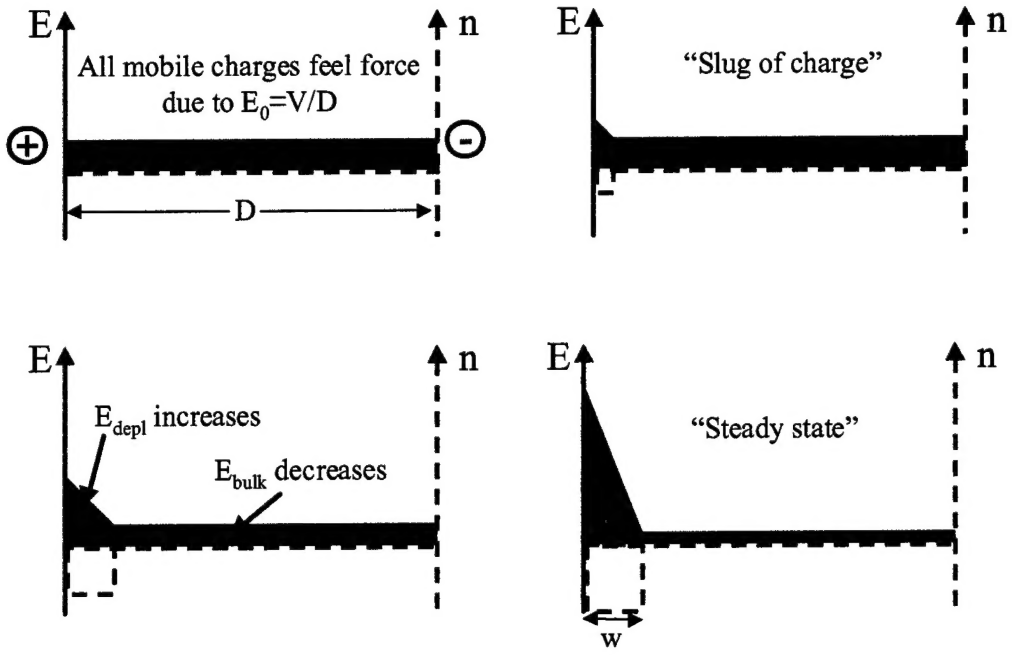

Figure 1. Simple model explaining the charge dynamics during the thermal poling process

immobile, negatively charged species such as non-bridging oxygen (NBO^-) hole centers. This charge density in the depletion region gives rise to an electric field, E_{depl}, which peaks at the anode surface of the glass sample. For longer poling times, the depletion layer electric field increases at the expense of the electric field in the bulk region. This process continues until most of the applied electric field drops across the depletion region (steady state condition). The steady state depletion layer width (w_0) is given by [16]

$$w_0 = \sqrt{\left(\frac{2\varepsilon V}{eN}\right)} \qquad \ldots (3)$$

where V is the applied poling voltage and N is the density of the mobile charges. Once the steady state condition is reached, if the sample is cooled down while the poling electric field is maintained, the electric field formed in the depletion layer can be

"frozen". Assuming a Na concentration of 1 ppm ($N=2x10^{16}$ cm^{-3}), the depletion layer width can be calculated to be ~10 μm, which in turn will give a peak electric field of ~10^7 V/cm. Such an electric field strength is very close to the nominal fused silica breakdown field strength of $3x10^7$ V/cm. Under the influence of this frozen-in electric field, there could be two different mechanisms which give rise to the observed second order nonlinearity viz. the $\chi^{(3)}E_{dc}$ effect or the reorientation of dipoles in the depletion region. Although the former effect seems to be consistent based on the estimated electric field (10^7 V/cm) and the known value of $\chi^{(3)}$ in fused silica (~10^{-22} m^2/V^2), one cannot discount the localized impurity model [8].

In the above model, it is assumed that only one cation species is the dominant mobile carrier that is responsible for the depletion layer formation. But, recently it has been found that the depletion region and the associated electric field are affected by injection of a secondary ionic species such as H^+ or H_3O^+ due to either surface moisture or the presence of OH species [17]. Furthermore, it has been shown that the nonlinear region in fused silica bulk samples is buried underneath the anode surface and moves towards the cathode logarithmically as a function of the poling time [18].

One of the key factors driving the research of poling in fused silica glass is the potential of extending the technology to fused silica optical fibers, the medium for optical communications. Poled fibers offer reduced insertion losses and lower packaging costs (associated with all-fiber devices), which are anticipated to be crucial for future communication systems. Our vision is that the integration of all-fiber devices such as

electro-optically tunable FBGs and waveplates with fiber lasers and amplifiers will enable advanced all-fiber laser sources such as modelocked lasers and tunable, narrow linewidth lasers.

Although the research on poled fused silica glasses has matured tremendously during the last decade, it has not been directly extendible to poled fibers. The key reason for this is that the mobile impurities responsible for the formation of the depletion region appear to be different in fibers. The dominant mobile impurity in fused silica glasses, Na, is not desirable for commercial optical fibers due to the scattering losses they induce in the important 1.55 μm telecommunications window. In the absence of Na impurities, the dominant mobile species in fibers are thought to be H^+ ions (due to OH content) or Ge-related defect sites [19]. However, more systematic studies need to be done to get a better understanding of the physical mechanisms behind fiber poling and thereby achieve second order nonlinearities as high as those achieved in bulk glasses.

There are several challenges related to the fabrication of poled fibers, which are not as severe or important in poled glasses. Two key issues are

- the overlap of the nonlinear region with the optical mode
- dielectric breakdown in the chosen poled fiber geometry

The overlap of the nonlinear region with the optical mode is a very interesting problem that involves a good understanding of the location and the width of the nonlinear region, and also the dynamics of the nonlinear region as a function of the poling time. According to the single carrier model, the peak of the nonlinear region is assumed to be at the anode

surface [16]. But, Alley et al [18] have clearly illustrated that the nonlinear region due to the fast carrier (such as K or Na) is at a certain depth from the anode surface and moves towards the cathode logarithmically as a function of the poling time. Can this model be extended to poled fibers also? If so, what is the fast carrier species and how does it behave at longer poling times? These are questions that require further research and attention, but unfortunately do not come under the scope of this dissertation.

The issue of dielectric breakdown in the chosen poled fiber geometry is important from the viewpoint of the maximum poling voltage that may be applied without causing electrical breakdown. From the discussion in the previous section, we know that the frozen-in electric field depends on the applied poling voltage, which determines the magnitude of the induced second-order nonlinearity. Typical thickness of fibers is in the order of 100 μm, which is approximately the separation distance between the two electrodes (if it is not polished to reduce its thickness). In air, the dielectric breakdown voltages are of the order of 500 V [20], which corresponds to an electric field of 5-10 V/μm. In previous literature [21], it has been stated that poling fields of >50 V/μm are needed to achieve an electro-optic coefficient of 0.3 pm/V. One possible solution is to perform the poling under vacuum. But, according to one reference [22], the breakdown fields were only 20 V/μm for distances of up to 1 cm even at 10^{-7} Torr. Another solution is to perform the poling in a high dielectric strength, high thermal stability medium such as silicone oil. But such a method is messy, cumbersome, and might introduce impurities into the fiber that modifies the poled fiber behavior. In our work, we used a high

dielectric strength (>100 V/μm) polyimide that was spin-coated around the fiber and baked to achieve proper insulation between the electrodes [21].

A.3. Tunable Poled Fiber Waveplates:

A key characteristic of poled silica fiber waveplates is that the magnitude of the second-order nonlinearity along the applied electric field (r_{33}) has been reported to be different from that along the perpendicular transverse direction (r_{31}) for poled fused silica bulk glass samples [8,16,23]. In fact, according to Kleinman symmetry conditions in transparent isotropic media such as fused silica glass [7], the relation between the two nonlinearities is predicted to be such that $\chi^{(3)}_{33}=3.\chi^{(3)}_{31}$. Since the quadratic nonlinearity is believed to have its origin in the built-in electric field interacting with the third-order susceptibility ($\chi^{(3)}$), the relation $r_{33}=3.r_{31}$ is plausible. Also, since the phase shift (ϕ) introduced by the poled section is directly proportional to the second-order nonlinearity (r) and the applied electric field (V/D) according to the relation,

$$\phi = \frac{\pi}{\lambda}.n^3 r \frac{V}{D}.L \qquad \ldots (4)$$

one should expect a voltage-induced birefringence from the poled section. If the applied voltage is such that the phase difference between the polarization along the direction of the electric field (along r_{33}) and the perpendicular polarization (along r_{31}) is π radians, a half-waveplate can be realized. The condition for such behavior can be deduced from Eq. (4) as

$$V_\pi = \frac{D}{L} \frac{\lambda_0}{n^3(r_{33}-r_{31})} \qquad \ldots (5)$$

where D is the thickness of the poled glass sample, L is the length of the poled section, and λ is the wavelength of the input light polarization. Similarly for a voltage of $V_{\pi}/2$, the poled fiber section can be used as a quarter-waveplate, as shown in Fig. 2. Assuming r_{33} = 0.3 pm/V, r_{31} = 0.1 pm/V, λ = 1.55 μm, D = 20 μm, L = 10 cm and n = 1.46, we get a $V_{\pi/2}$ voltage of 250 V. A key challenge in the demonstration of an all-fiber waveplate is to measure the relative magnitudes of r_{33} and r_{31} for poled fibers. This issue and other issues related to the all-fiber waveplate demonstration are discussed in the following sub-sections.

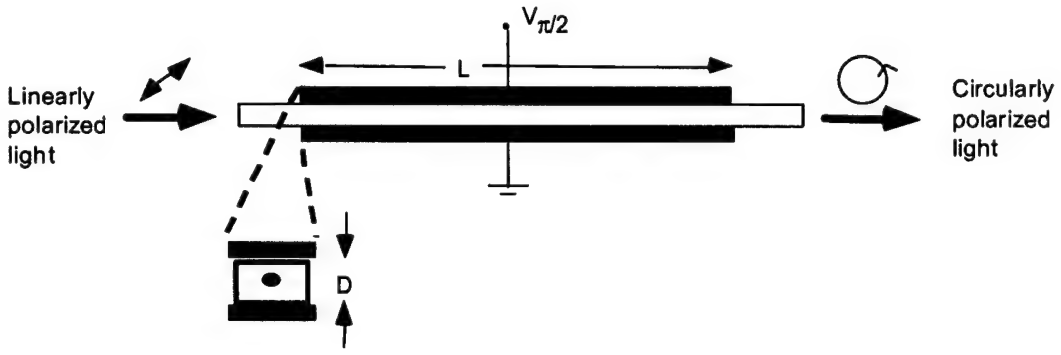

Figure 2. Schematic diagram of a poled fiber section illustrating quarter-waveplate operation

B. Custom Fiber Design

Commercially available fibers are not well suited for fabricating poled fiber segments. One choice for this application is the D-shaped fiber available from KVH Corporation. Even in this case, the flat side of the D-shaped fiber has to be polished down to proximity of the core (~5 μm) before it is suitable for poling. Such polishing steps are cumbersome and can introduce micro-scratches on the fiber that make the fiber fragile, and eventually contribute to low yield for poled fiber fabrication. Another issue is that of

the dopants used in the commercially available fibers. As discussed in Sec. A.2, we know from bulk glass studies that dopants like Na^+, K^+ and Li^+ enable the formation of the depletion region and therefore is responsible for the built-in electric field. But, such dopants are found in negligible quantities in fibers. As such, there is a strong need for *developing specialty custom fibers* for use in poling.

In practice, the two key fiber design parameters that are most significant in tailoring the magnitude of the effective second-order nonlinearity are: (i) the thickness of the fiber, and (ii) the distance of the anode from the center of the fiber core. The thickness of the fiber is important from the viewpoint of the breakdown voltage of the electrode structure during poling. As discussed in Sec. A.2, the larger the poling voltage, the larger the built-in electric field and hence a large second-order nonlinearity may be obtainable. Kazansky et al [24] have reported a breakdown electric field of ~1000 V/μm for their germanosilicate glass fiber. However, in their case, they used a twin-hole structure in the cladding wherein the electrodes inserted into the holes were surrounded by glass. Although such a fiber design is optimum for poling, the insertion of the wires is a cumbersome step and splicing the fiber to other fiber components is difficult. Good poling results have also been demonstrated at UNM [21] by spinning several layers of polyimide around the fiber to provide for insulation between the electrodes. However, the breakdown field strength of the polyimide is only 300 V/μm [25], a value that is much lower than that of the glass itself. In our experiments, imperfect surfaces, dirt, and non-optimal baking procedures limit the breakdown strength further down to 200 V/μm.

Assuming this value of the breakdown field strength, the distance between the electrodes on the fiber should be at least of the order of 20 μm to facilitate poling at >5 kV.

The other issue that contributes to optimization of the second-order nonlinearity is the distance between the fiber surface where the anode is located and the center of the fiber core. This parameter is critical in determining the overlap of the nonlinear region and the optical mode propagating primarily in the core of the fiber. From bulk glass studies, based on the single carrier model, we know that the peak of nonlinear region is typically located close to the anode surface [8]. This assumption has been modified by Alley et al [18] in their two-carrier model, which predicts that at least one of the carriers causes the nonlinear region to move towards the cathode logarithmically with respect to poling time. However, such a model has not been validated for the case of poled fibers and had been one of the goals of this dissertation. Based on previous reports [21,26], we fixed the core to anode surface distance as 5 μm.

Other considerations related to the design of the custom fiber are the core diameter (2a) and the numerical aperture (NA), which are related to the characteristic parameters of waveguides, viz. the V number and the mode field diameter (MFD) by [27]

$$V = \frac{2\pi a}{\lambda}.NA \qquad \ldots (6)$$

$$MFD = 2a.\left(0.65 + \frac{1.619}{V^{1.5}} + \frac{2.879}{V^{6}}\right) \qquad \ldots (7)$$

Our fiber was designed to be singlemode at 1550 nm. In order to minimize the losses due to evanescent field radiation, the optical mode should be tightly confined. With this in mind, an assumed core diameter of 7 μm, and a mode confined to a mode field diameter of 8 μm, we deduce a value of 2.412 for the V number from Eq. (6), and thereby a value of 0.17 for the numerical aperture from Eq. (5). In summary, the specifications of the custom fiber (see Fig. 3) were:

Fiber dimension	= 20 μm (D) x 125 μm (A)
Core diameter	= 7 μm
Core location	= 5 μm (d) from one of the flat surfaces (Fig. 3)
Numerical aperture	= 0.17

Furthermore, the fiber was specified to be doped with 1 ppm Na to enhance the second order nonlinearity based on the results of Kazansky et al [19].

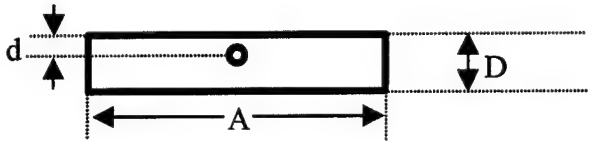

Figure 3. Schematic diagram of the cross-section of custom ribbon fiber

C. Issues Related to Poled Fiber Waveplates

The key issues related to the achievement of poled fiber waveplates are: (1) large differences in the magnitudes of r_{33} and r_{31}, and (2) depolarization effects due to (i) mode scattering, (ii) polarization dependent attenuation, and (iii) polarization mode dispersion.

C.1. Relative magnitudes of r_{33} and r_{31}

There have been several contradictory reports regarding the relative magnitudes of r_{33} and r_{31} in poled waveguides. As mentioned in Section A., early reports [8,16,23] on the relative magnitude of the nonlinearities seemed to indicate a ratio of close to 3, which is consistent with the predicted values from Kleinman symmetry conditions. This observation was further validated for poled fiber sections by Long et al [21], who measured the ratio of the nonlinearities (r_{33}/r_{31}) to be ~2.4. However, recent reports [28,29] suggest that this ratio may be close to unity.

One possible reason for the measurement of a ratio much lesser than 3 is the electrostrictive effect in fibers, which has been found to be significant for frequencies up to 200 MHz in fibers [30]. The electrostrictive effect manifests itself in fibers through the strain-optic coefficients, which for silica has been measured to be ρ_{11}=0.11 (along the direction of the applied electric field) and ρ_{21}=0.27 (perependicular to the applied electric field) [31]. As such, the electrostrictive effect counters the electro-optic effect, and at low frequencies where this effect is strong, it may lead "measured ratios" that are less than the value of 3 predicted from Kleinman symmetry conditions and may be the reason for the weak polarization dependence measured by other workers [28,29]. However, since the electrostrictive effect is strongly dependent on the frequency and the device geometry, its contribution should be subtractable for appropriately chosen poled fiber designs and frequencies of measurement.

Another issue is based on an interesting observation by Kielich [32] in his classic paper in 1969. In that paper, it was suggested that the ratio of 3 exists in homogeneously poled isotropic media under two limiting cases: (1) when the poling field is low, and (2) when the nonlinearity is solely caused by an internal space-charge field and no dipoles are aligned to the poling field. Such an observation is consistent with the results of poled glass studies, where the poling field is indeed low. But, for the case of thin films and fibers, where the poling fields are much larger, the anticipated ratios can be as low as unity [32]. This issue needs to be investigated further through detailed studies in poled fibers.

C.2. Depolarization effects in fibers

Depolarization in fibers is an important issue that may hinder the electro-optic waveplate operation. As mentioned above, the typical sources of depolarization in fibers are spurious birefringences due to imperfections in the fiber, mode scattering, proximity of metal surface and polarization mode dispersion. One method of reducing the problem of spurious birefringence is to use highly birefringent fibers. But, since the beat length of such fibers is in the order of millimeters, uncompensated poled fiber devices (which are on the order of fraction of a meter in length) would lead to multiple order devices with limited bandwidths of operation. The latter problem could be solved by using two near-equal lengths of highly birefringent fibers with a 90° rotation between the two pieces to yield a "compensated" section.

(i) Mode Scattering: The issue of depolarization due to mode scattering is critical in fibers which support more than one mode in their core. Such was the case for our initial experiments wherein we launched 633 nm light into poled fiber sections based on our 1550 nm custom ribbon fiber. This was done partly due to the easy availability of polarization optics at 633 nm and for experimental convenience. We observed very poor degree of polarization (<20%) at the output of the poled fiber. This can be explained using the model of Ramaswamy et al [33] in which the normalized birefringence (Y) can be expressed as

$$Y = \left(1-\varepsilon^2\right)\frac{3\pi^2 V^2}{(V+2)^4} \qquad \ldots (8)$$

where the aspect ratio, ε = b/a (the ratio of the minor axis dimension over the major axis dimension). Using Eq. (8), the normalized birefringence as a function of the fiber V number for different elliptical core aspect ratios is plotted in Fig. 4. As we can see from

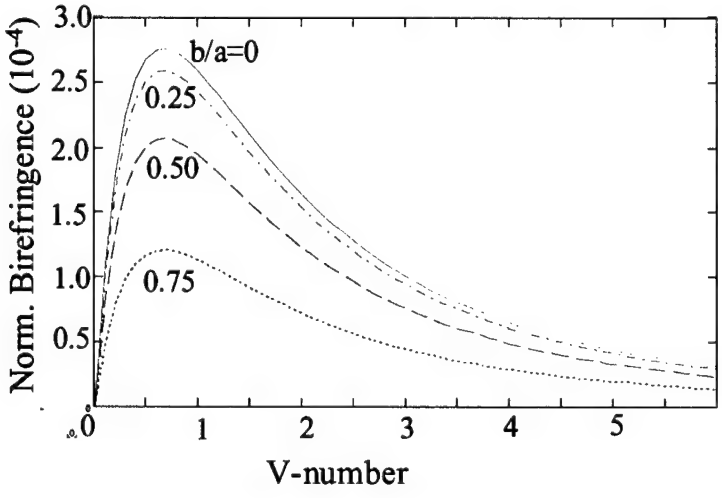

Figure 4. Calculated plot of the normalized birefringence as a function of the fiber V number

the plot (courtesy, T. Thompson), for large V numbers (multimode regime) the birefringence degrades rapidly and hence the degree of polarization degrades rapidly. This effect is more prominent for a highly birefrient fiber (b/a=0) than for a ciruclar core fiber (b/a=1). *The above result implies that the fibers used for the waveplate demonstration should be strictly single mode, which is very easy to achieve in practice.*

(ii) Polarization-Dependent Attenuation: Another issue that contributes to the degradation of the degree of polarization is polarization-dependent attenuation. This issue can be analyzed using the four-layer slab model described in Adams [34], which consists of three dielectric layers (cladding, core, and cladding) and a metal layer. The presence of the metal impacts the propagation constant of the TM mode significantly more than that of the TE mode. This can be attributed to the deeper penetration of the TM mode into the metal as a result of the surface plasma-like behavior of the TM mode at the metal-dielectric interface. One way of expressing the depolarization is the polarization-dependent loss, which can be calculated based on the model of Adams in which the loss per unit length for either the TM or TE mode is expressed as

$$\alpha = \frac{2(N+1)^2\pi^2}{(2a)^3 k n_1}\left(\frac{\eta_{23}}{\eta_{12}}\right)\left[\frac{2\beta_3}{\left(\eta_{23}^2\beta_3^2+\beta_2^2\right)\cosh(4d\beta_2)+\left(\eta_{23}^2\beta_3^2-\beta_2^2\right)}\right] \quad \ldots (9)$$

where

$$\eta_{ij} = 1 \quad \text{for TE modes}$$

$$= n_i^2/n_j^2 \quad \text{for TM modes}$$

The suffix 1 corresponds to the core layer, suffices 2 and 4 correspond to the cladding layers on either side of the core and suffix 3 corresponds to the metal layer. The β_i are the propagation constants and d is the distance between the metal layer and the center of the core. Using Eq. (9), we can determine the polarization-dependent loss as a function of the metal layer distance 'd'. Such a plot is shown in Fig. 5 for the case of a Au metal layer on a KVH 633 nm D-shaped fiber. From the plot, one sees that the polarization dependent loss for a poled fiber length of 10 cm is negligible even for distances of 4.5 μm from the center of the fiber core. *This implies that the fiber could be polished down to 5 μm from the center of the fiber core and poled without degrading the performance of the waveplate signficantly.*

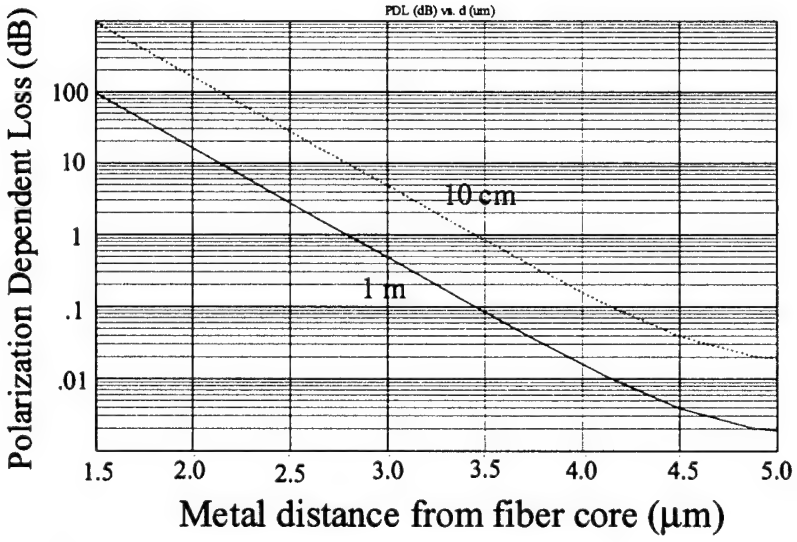

Figure 5. Plot of the polarization dependent loss (in dB) as a function of the distance of the metal layer from the center of fiber core

(iii) Polarization Mode Dispersion: When monochromatic light is used, the birefringence in a fiber introduces a phase delay between the two polarization eigenmodes. This causes the state of polarization to change when both modes are excited,

without affecting the degree of polarization. However, when non-monochromatic light is guided, the polarization state changes are superimposed upon a reduction in the degree of polarization due to the group delay difference between the two modes [1]. This group delay time difference per unit length is called the *polarization mode dispersion.* If only one polarization eigenmode is excited, both the state and degree of polarization is unchanged along the fiber, regardless of the bandwidth of light. Depolarization occurs in a fiber only if both modes are excited with light of finite bandwidth.

The polarization mode dispersion (PMD) can be calculated directly from the birefringence dependence of the fiber on the V-number according to the relation [35]

$$\Delta t = \frac{L}{c}\left[\Delta\ddot{\beta} + V.\frac{\partial(\Delta\ddot{\beta})}{\partial V}\right] \qquad \ldots (10)$$

where L is the length of the fiber and c is the velocity of light. Using this expression, we plotted the PMD as a function of the V number for a 10 cm long fiber which had a 2:1

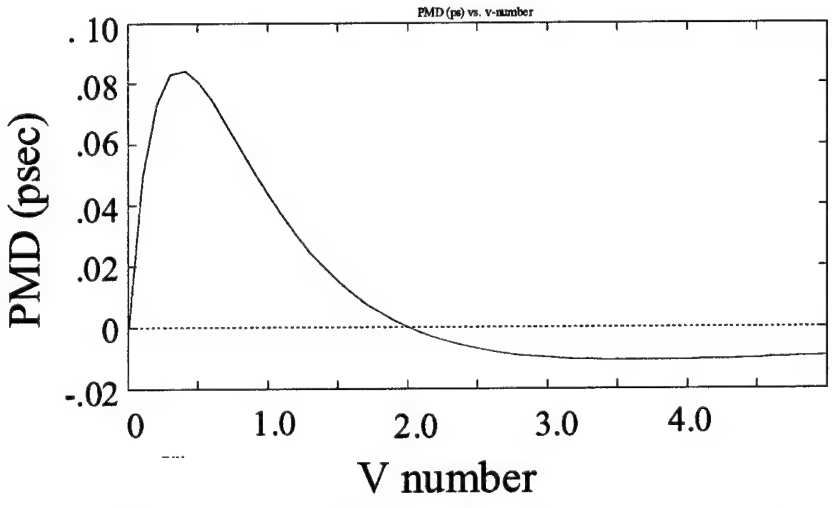

Figure 6. A plot of the difference in the group index between the two polarization eigenmodes as a function of fiber V number

elliptical core (such as the 633 nm D-shaped fiber used in our experiments). From the plot of Fig. 6, we can see that PMD is negligible around the single mode regime. This is because the normalized birefringence does not vary strongly as a function of the V number in this regime (as might be obvious from Fig. 4). For V numbers much lower than 2 (longer wavelengths), the normalized birefringence is a strong function of the V number and hence the PMD is high. *The above result implies that depolarization due to PMD is negligible if we use single-mode fibers.*

D. Experiments and Results

One of the goals of this program was to demonstrate all-fiber waveplates at 1550 nm using poled fiber sections. Towards this end, we designed and ordered a custom ribbon fiber. However, fabrication of a ribbon fiber with a high aspect ratio (~6:1, 125μmx20μm) is difficult due to surface tension, which tends to make the fiber shape circular. Also, since the thermal expansion coefficient of the core is slightly different than that of the cladding, the core tended to become elliptical while drawing. Because of these

Figure 7. Cross-section of our custom ribbon fiber

factors, the fiber we obtained was not flat (slightly bow-shaped) and more importantly, the elliptical core (visible as a bright spot on the lower middle portion of the fiber cross-section shown in Fig. 7) was situated such that the evanescent field extended out to the flat surface of the fiber. This resulted in high losses at 1550 nm (~9 dB for a 10 cm long fiber) and significant depolarization (<30% degree of polarization a the output). Preliminary experiments using a ribbon fiber poled at 2.2 kV at 260°C for 20 minutes yielded a r_{33} of ~0.03 pm/V (measured using a Mach-Zehner interferometer with a $LiNbO_3$ reference [21]). Such a low electro-optic coefficient is presumably due to a non-optimal overlap of the nonlinear region and the optical mode. We also applied voltages of up to 1 kV across the sample and did not observe any polarization rotation. This is probably due to the poor degree of polarization at the output. For these reasons and due to the fact that V_π is directly proportional to the wavelength of light used, we decided to use 633 nm D-shaped fibers for our experiments.

A key feature of our experiments is the use of the Mueller matrix method [36] to characterize the retardation as a function of the applied voltage. One of the issues that needed to be resolved in the demonstration of a poled fiber waveplate is the magnitude of the electrostrictive effect for our poled fiber structure. An experiment that can clearly indicate the phase shift due to electrostriction is to measure the phase shift before and after a fiber is poled. We fabricated a D-shaped fiber sample for this experiment and measured the phase shift for an applied voltage of 5 V in a Mach-Zehnder interferometer. Negligible phase shift was observed (buried under noise level). Then we poled the same fiber sample at 800 V and we were able measure a phase shift that was two orders of

magnitude above than the noise level. Such a result clearly indicates that the contribution to the phase shift from our poled fiber samples due to electrostriction was negligible.

The second order nonlinear coefficient (r) observed for the above fiber sample was less than 0.01 pm/V. This was due to the relatively low poling voltage (800 V) used. The poling voltage was limited by the electrode pattern on the flat side of the fiber extending out to the edges (due to lithography process errors). In a subsequent experiment, another sample was fabricated using the 633 nm D-shaped fiber. Unlike the previous fiber sample, the stripline electrode fabricated on this sample was well defined (~30 μm wide over 70 mm) and continuous. This facilitated the use of a voltage up to 1500 V for poling the sample. The resultant second order nonlinearity (r_{33}) induced in the sample was 0.04 pm/V. The sample was then placed in the waveplate characterization setup to measure the retardation as a function of the applied voltage. Assuming $r_{33}=3.r_{31}$, the sample should exhibit quarter-wave retardation for a voltage of 2.5 kV. But even for an applied voltage of 1.5 kV (we did not want to use higher voltages in order to prevent electrical breakdown), there was no measurable retardation observed. This could be due to two reasons viz. (1) the ratio r_{33}/r_{31} is much less than 3, or (2) the nonlinear region does not overlap the fiber core optimally. The relative contributions of r_{33} and r_{31} can be measured directly using a stable Mach-Zehnder interferometer in which the polarization of the input light can be manipulated appropriately. Unfortunately, such an interferometer was not available at the time of this experiment.

Future experiments should attempt to measure the relative contributions of r_{33} and r_{31} as a function of the poling voltage as well as the poling time. Such data will provide the poling conditions that are optimal for achieving a ratio (r_{33}/r_{31}) of much greater than unity and an optimal overlap of the nonlinear region with the fiber core, thus paving the way for the demonstration of efficient electrically-tunable all-fiber waveplates.

E. References

1. S.C. Rashleigh, "Origins and Control of Polarization Effects in Single-Mode Fibers", Jour. Lightwave Technol. **LT-1**, 312 (1983)

2. R. Ulrich, "Polarization Stabilization on Single-Mode Fiber", Appl. Phys. Lett. **35**, 840 (1979)

3. F. Heismann, "Integrated-Optic Polarization Transformer for Reset-Free Endless Polarization Control", IEEE Jour. Quantum Electron. **25**, 1898 (1989)

4. T. Kawazoe, K. Satoh, I. Hayashi, and H. Mori, "Fabrication of Integrated-Optic Polarization Controller Using Z-Propagating Ti-$LiNbO_3$ Waveguides", Jour. Lightwave Technol. **10**, 51 (1992)

5. R. Ulrich, S.C. Rashleigh, and W. Eickhoff, "Bending Induced Birefringence in Single Mode Fibers", Opt. Lett. **5**, 273 (1980)

6. H.C. Lefevre, "Single-Mode Fractional Wave Devices and Polarization Controllers", Electron. Lett. **16**, 778 (1980)

7. R.W. Boyd, "Nonlinear Optics", Academic Press (1992)

8. R.A. Myers, N. Mukherjee, and S.R.J. Brueck, "Large Second-Order Nonlinearity in Poled Fused Silica", Opt. Lett. **16**, 1732 (1991)

9. T. Fujiwara, D. Wong, Y. Zhao, S. Fleming, V. Grishina, and S. Poole, "Electro-Optic Modulation in Germanosilicate Fiber with UV-Excited Poling", Electron. Lett. **31**, 573 (1995)

10. A. Okada, K. Ishii, K. Mito, and K. Sasaki, "Phase-Matched Second-Harmonic Generation in Novel Corona Poled Glass Waveguides", Appl. Phys. Lett. **60**, 2853 (1992)

11. P.G. Kazansky, A. Kamal, and P.St.J. Russell, "High Second-Order Nonlinearities Induced in Lead Silicate Glass By Electron-Beam Irradiation", Opt. Lett. **18**, 693 (1993)

12. M. Ohama, T. Fujiwara and A.J. Ikushima, "Decay of Ultraviolet-Induced Optical Absorption in Ge-Doped SiO_2 Glass", Appl. Phys. Lett. **73**, 1481 (1998)

13. T. Fujiwara, M. Takahashi, and A.J. Ikushima, "Decay Behavior of Second-Order Nonlinearity in GeO2-SiO_2 Glass Poled With UV-Irradiation", Electron. Lett. **33**, 980 (1997)

14. A. Okada, K. Ishii, K. Mito, and K. Sasaki, "Second-Order Nonlinearity in Corona-Poled Glass Films", J. Appl. Phys. **74**, 531 (1993)

15. H. Imai, S. Hironouchi, Y. Uchida, H. Yamasaki, K. Fukao, G. Zhang, T. Kinoshita, K. Mito, H. Hirashima, and K. Sasaki, "Time-Dependent Decay of Quadratic Nonlinearity in Corona-Poled Silicate Glass Films", J. Non-Cryst. Solids **196**, 63 (1996)

16. P.G. Kazansky and P.St.J. Russell, "Thermally Poled Glass: Frozen-In Electric Field or Oriented Dipoles?", Optics Commn. **110**, 611 (1994)

17. T.G. Alley, S.R.J. Brueck, and R.A. Myers, "Space Charge Dynamics in Thermally Poled Fused Silica", J. Non-Crystalline Solids **242**, 165 (1998)

18. T.G. Alley, and S.R.J. Brueck, "Visualization of the Nonlinear Optical Space-Charge Region of Bulk Thermally Poled Fused-Silica Glass", Opt. Lett. **23**, 1170 (1998)

19. P.G. Kazansky, P.St.J. Russell, and H. Takebe, "Glass Fiber Poling and Applications", Jour. Lightwave Technol. **15**, 1484 (1997)

20. J.M. Meek and J.D. Craggs, "Electrical Breakdown of Gases", John Wiley (1978)

21. X-C. Long, R.A. Myers, and S.R.J. Brueck, "A Poled Electrooptic Fiber", IEEE Photon. Technol. Lett. **8**, 227 (1996)

22. V.N. Maller and M.S. Naidu, "Advances in High Voltage Insulation and Arc Interruption in SF6 and Vacuum", Pergamon Press (1981)

23. X-C. Long, R.A. Myers, and S.R.J. Brueck, "Measurement of the Linear Electro-Optic Coefficient in Poled Amorphous Silica", Opt. Lett. **19**, 1819 (1994)

24. P.G. Kazansky, A.R. Smith, L. Dong, P.St.J. Russell, "Second-Harmonic Generation in Silica Fibers Poled Via Internal Electrodes, Conference of Lasers and Electro-Optics (CLEO) Technical Digest, paper CWK2, pp. 310 (1996)

25. Toray America Inc., PhotonEECE UR3 140 polyimide specification sheet

26. B. Srinivasan and R.K. Jain, "First Demonstration of Thermally Poled Electrooptically Tunable Fiber Bragg Gratings", IEEE Photon. Technol. Lett. 12, 170 (2000)

27. E.G. Neumann, Single Mode Fibers, Springer (1990)

28. A.C. Liu, M.J.F. Digonnet, and G.S. Kino, "A DC Kerr Measurement in a Silica Channel Waveguide", Proc. SPIE, **2841**, 209 (1996)

29. J. Arentoft, K. Pederson, S.I. Bozhevolnyi, M. Kristensen, and P. Yu, "Weakly Polarization Dependent Electro-Optic Effect in Poled Silica", Bragg Gratings and Photosensitivity Conference Technical Digest, paper ThE17, pp. 96 (1999)

30. E.L. Buckland and R.W. Boyd, "Measurement of the Frequency Response of the Electrostrictive Nonlinearity in Optical Fibers", Opt. Lett. **22**, 676 (1997)

31. W. Primak and D. Post, "Photo-elastic Constants of Vitreous Silica and its Elastic Coefficient of Refractive Index", J. Appl. Phys. **30**, 779 (1959)

32. S. Kielich, "Optical Second-Harmonic Generation by Electrically Polarized Isotropic Media", IEEE J. Quantum Electronics, **5**, 562 (1969)

33. V. Ramaswamy, W.G. French, and R.D. Standley, "Polarization Characteristics of Non-Circular Single Mode Fibers", Applied Optics, **17**, 3014 (1978)

34. M.J. Adams, "Introduction to Optical Waveguides", Macmillan (1981)

35. R.B. Dyott, "Elliptical Fiber Waveguides", Artech (1995)

36. E. Collett, "Polarized Light: Fundamentals and Applications", Dekker (1992)